analytical chemistry

Article

Cite This: Anal. Chem. 2018, 90, 2517−2525

pubs.acs.org/ac

Validity of Measuring Metallic and Semiconducting Single-Walled Carbon Nanotube Fractions by Quantitative Raman Spectroscopy

Ying Tian,*[,†,‡] Hua Jiang,*[,‡] Patrik Laiho,[‡] and Esko I. Kauppinen[‡]

[†]Department of Physics, Dalian Maritime University, Dalian, Liaoning 116026, China

[‡]Department of Applied Physics, Aalto University School of Science, Puumiehenkuja 2, 00076 Aalto, Finland

Supporting Information

ABSTRACT: Although it is known that the Raman spectroscopic signature of single-walled carbon nanotubes (SWCNTs) is highly chirality dependent, using Raman spectroscopy with several laser excitations as a tool for quantifying fraction of either metallic or semiconducting nanotubes in a sample has become a widely used analytical method. In this work, using the electron diffraction technique as a basis, we have examined the validity of Raman spectroscopy for quantitative evaluation of metallic fractions (M%) in single-walled carbon nanotube samples. Our results show that quantitative Raman spectroscopic evaluations of M% by using several discrete laser lines, either by using integrated intensities of chirality-associated radial breathing modes (RBMs) or, as has been more commonly utilized in recent studies, by statistically counting the numbers of RBMs can be misrepresentative. Specifically, we have found that the occurrence numbers of certain types of RBMs in Raman spectral mapping depend critically on the diameter distribution, resonant coupling between transition energies and excitation laser energy, and the chirality-dependent Raman scattering cross sections rather than simply on the metallic and semiconducting SWCNT fractions. These dependencies are similar to those observed in the integrated intensities of RBMs. Our findings substantially advance the understanding of the proper use of Raman spectroscopy for carbon nanotube quantification, which is important for carbon nanotube characterization and crucial to guide research in SWCNT growth and their applications.

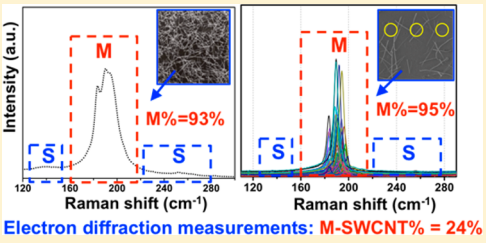

Single-walled carbon nanotubes (SWCNTs) are one of the most promising candidates for future high-performance electronic devices because of their remarkable physical, mechanical, and electrical properties.[1−5] A SWCNT can be either metallic (M) or semiconducting (S) depending on its chirality, usually denoted by a pair of integers (n,m), that is, M-SWCNT when $mod(n - m, 3) = 0$ and S-SWCNT if $mod(n - m, 3) = 1$ or 2 (commonly referred to as *mod1* or *mod2* types, respectively).[6] M-SWCNTs can withstand ultrahigh current densities due to ballistic electron transport,[7,8] while S-SWCNTs possess high intrinsic carrier mobility and are an ideal channel material for field-effect transistors.[1] In spite of their extraordinary electrical properties, an as-prepared sample usually contains a mixture of M- and S-SWCNTs, which significantly degrades the device performance and causes serious nonuniformity.[5] Therefore, over the past decade, tremendous efforts have been devoted to obtaining SWCNTs of a uniform electrical type or even a single chirality, either by direct synthesis techniques with optimized growth conditions[5,9−13] or by postsynthesis separation protocols, such as density gradient centrifugation[14] or DNA assisted separation of SWCNTs.[15,16] Along with those efforts, there is an urgent demand for accurate, efficient, and fast methods to measure the fractions of M- (M%) or S-SWCNTs (S%) in samples, which is critical for providing feedback to further correctly guide the experiments and to accelerate the commercialization of carbon nanotube materials.

Among a number of characterization methods, Raman spectroscopy is one of the most popular tools for SWCNT structure measurements. It requires minimal sample preparation but provides a wealth of information about the quality of the material, the conductivity and chiral structure of the nanotubes, and their phonon and electron quantum confinement.[17] Recently Raman spectroscopy at discrete multiple laser excitations has become a commonplace tool to quantify a fraction of a specific type of conductivity[9−11,18−30] or even the population of nanotubes of a certain chirality in the as-grown SWCNT samples.[10,11,31,32] In the reported quantitative evaluation procedures, two strategies are used to calculate the M% or S% in a sample. Both approaches are based on the radial breathing modes (RBM) features of resonant (n,m) SWCNTs, either by calculating the integrated RBM intensities[18−24] or by statistically counting the number of RBM peaks[25−33] appearing in the regions of Raman spectra assignable to M- and S-SWCNTs. Both methods take for granted that the integrated intensities or the occurrences of RBMs positioned in the M- and S-SWCNT regions of Raman spectra are simply proportional to the M- and S-SWCNT abundance in the sample. However, Raman scattering in SWCNTs is a resonant process. The appearance of an RBM and its intensity depend largely on

Received: September 11, 2017
Accepted: January 16, 2018
Published: January 16, 2018

DOI: 10.1021/acs.analchem.7b03712
Anal. Chem. 2018, 90, 2517−2525

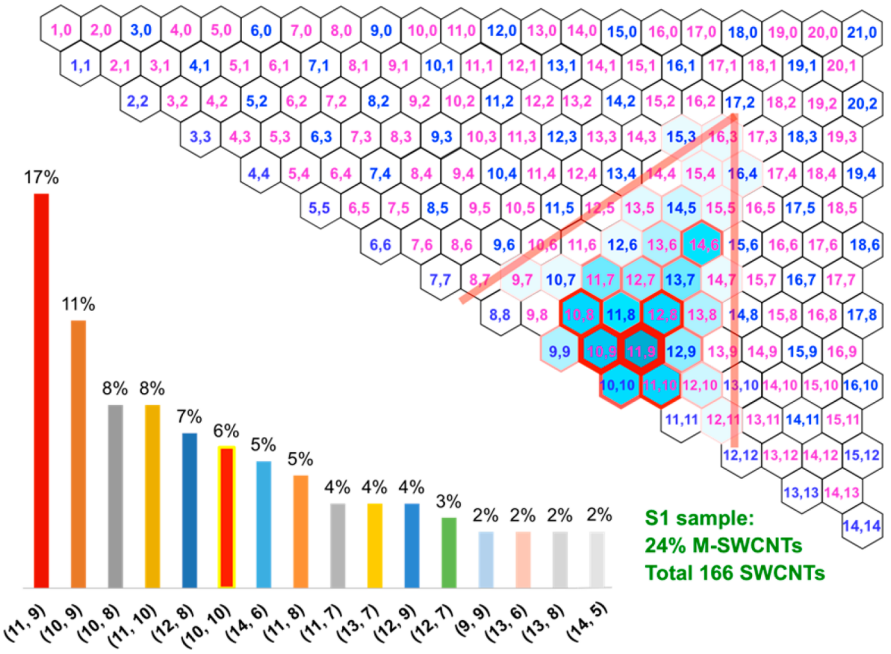

Figure 1. Chirality map of sample S1 acquired from ED analysis of 166 individual SWCNTs. For simplicity, the histogram plots only nanotubes with occurrence rate more than 2%. The very narrow (n,m) distribution of S1 is gathered at the armchair region with (11,9) being the most abundant chirality. The M% of S1 is 24%, and narrow diameters distribution falls into the 1.2−1.5 nm range.

the match of transition energies (E_{ii}) with excitation laser energy (E_{Laser})[34−36] as well as environment[37−39] and SWCNT (n,m) structure.[40−46] These facts cast shadows over experimental quantitative or even qualitative analysis of M% using RBM features from Raman spectra measured at discrete multiple E_{Laser}.

Here we present a thorough study of the validity of current practices using Raman spectroscopy for quantitative assessment of the fraction of metallic or semiconducting carbon nanotubes. Three SWCNT samples with different diameter distributions were involved in the study. First, we obtained the (n,m) distribution maps and M% of all three samples using a microbeam electron diffraction (ED) technique. The M% of the same samples were then investigated using Raman spectroscopy. Two common practices of Raman characterization were examined: (1) by analyzing the integrated RBM intensities of Raman spectra measured from thin films and (2) by statistically counting the RBM numbers of hundreds of micro-Raman spectra in Raman spectral mapping acquired from SWCNTs on a substrate. By discerning the difference of Raman outcomes from the ED results, we have a multidimensional perspective on a number of issues associated with current approaches of Raman quantitative analysis of M% and chirality population. Those important findings pave the way to reliable measurements of M- and S-SWCNT fractions with quantitative Raman spectroscopy and further guide SWCNT experiments for their various promising applications.

EXPERIMENTAL SECTION

SWCNT Samples. Three SWCNT samples were studied in this work, including two SWCNT samples synthesized by the floating catalyst-chemical vapor deposition (FC-CVD) methods,[47,48] and a commercial RM8281 SWCNT reference material released by the U.S. National Institute of Standards and Technology (NIST).[49,50] For convenience, these samples are referred to as S1 (synthesized by FC-CVD with ferrocene as catalyst precursor[47]), S2 (synthesized by FC-CVD with spark discharge generated Fe particles as catalysts[48]), and RM8281 (reference material from NIST). The diameter distributions of S1, S2, and RM8281 samples are 1.2−1.5, 0.8−1.4, and 0.7−0.9 nm, respectively. In addition, a commercial purified high-pressure CO disproportion (HiPCO) SWCNT powder (batch, HP27-061C, NanoIntegris Inc.) with a diameter distribution of 0.8−1.2 nm was used as a reference SWCNT sample, with an assumed M% of 36 (±4)%[9,18−20,23] to calculate the M% of an unknown SWCNT sample using integrated RBM intensities.

Transmission Electron Microscopy and Electron Diffraction. High-resolution transmission electron microscope (TEM) imaging and electron diffraction measurements were carried out by using a JEOL-2200FS double aberration-corrected microscope (JEOL Ltd., Japan), operated at 80 kV, well below the electron knockout damage threshold for carbon.[51] For electron diffraction analysis, TEM samples were so well prepared that SWCNTs were well dispersed on holey carbon film supported TEM grids, and only isolated and straight SWCNTs were analyzed. Determination of the chiral indices (n,m) from electron diffraction patterns of individual SWCNTs was based on a calibration-free intrinsic layer line-spacing method.[52]

Raman Spectroscopy. Raman spectra of all SWCNT samples were performed on a Labram-HR 800 (Horiba Jobin-Yvon) Raman spectrometer by using four laser wavelengths (λ_{Laser}) of 488, 514, 633, and 785 nm. The Raman spectrometer is coupled with a Synapse 1024 × 256 thermoelectrically cooled open-electrode charge coupled device (CCD) detector (Horiba) and an Olympus BX-41 microscope equipped with 10×, 20×, 50×, and 100× magnification objectives. A PC controlled XYZ stage with a scan area of 75 mm × 50 mm ($X \times Y$) and step size of 100 nm allows automated acquisition of Raman spectral mapping measurements. An 1800 mm^{-1} grating was utilized to obtain a high spectral resolution of 1 cm^{-1}.

DOI: 10.1021/acs.analchem.7b03712
Anal. Chem. 2018, 90, 2517−2525

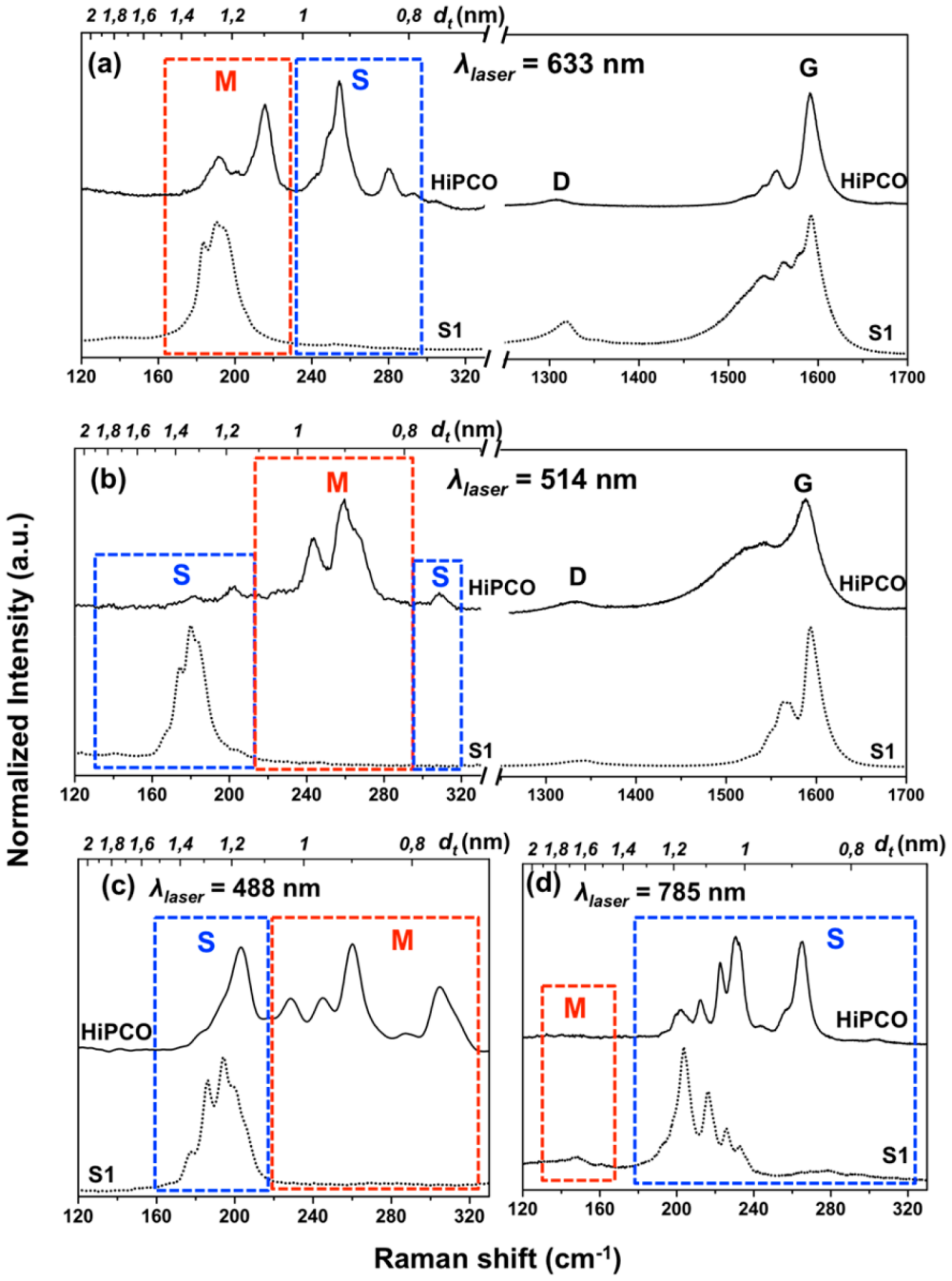

Figure 2. Raman spectra of the S1 and HiPCO samples excited by four λ_{Laser}. RBMs and G,D bands at λ_{Laser} of (a) 633 and (b) 514 nm and RBM Raman spectra at λ_{Laser} of (c) 488 and (d) 785 nm, respectively. The blue and red dashed squares correspond to the RBM regions assignable to S- and M-SWCNTs, respectively. The RBMs measured from the S1 sample correspond to mainly M-SWCNT at λ_{Laser} = 633, while only S-SWCNT at λ_{Laser} = 488, 514, and 785 nm.

For the SWCNT thin film and powder samples, the Raman spectrum is averaged based on the measurements of three different points of each sample, and the 50× microscope objective was used to cover a larger area of the sample. For the Raman spectral mapping measurements, we directly deposited S1 sample onto Si/SiO_2 chips from the FC-CVD reactor using a thermophoretic precipitator[53] with a controlled tube density of ∼2 tubes/μm. The average tube length of S1 is ∼3 μm. It is worth noting that the length of SWCNTs is an essential parameter to be considered in the Raman spectral mapping measurement, since the RBM from the same nanotube could be multiply counted if the scanning step is smaller than the nanotube length. Therefore, to avoid multiple counting of RBMs from the same SWCNT, the Raman spectral mapping was recorded by scanning the S1 sample on substrate surface in the area of 60 μm × 60 μm with a scanning step of 4 μm and a laser spot diameter of ∼1 μm through the 100× objective. All Raman spectral mapping measurements at the four λ_{Laser} were performed at the same locations, which in total resulted in 1024 micro-Raman spectra. The M% calculation uncertainty is about ±10%, which is estimated from the spectral fitting of obtaining integrated RBM intensity or from counting the numbers of RBMs in Raman spectral mapping.

DOI: 10.1021/acs.analchem.7b03712
Anal. Chem. 2018, 90, 2517−2525

Scanning Electron Microscopy. Scanning electron microscopy (SEM, Zeiss Sigma VP) was used to measure the density and lengths of SWCNTs on Si/SiO_2 wafers, which were deposited directly from the FC-CVD reactor.

RESULTS AND DISCUSSION

Electron Diffraction Characterization. We measured the chirality distributions of three samples, denoted S1, S2, and RM8281, using ED. To determine the chirality of an individual SWCNT, a high-quality diffraction pattern with enhanced signal-to-noise ratio is needed. Figure S1 (see the Supporting Information) shows an example of such electron diffraction patterns accompanied by a corresponding TEM micrograph of an isolated SWCNT. The diffraction pattern is mainly composed of a set of parallel-diffracted layer lines that are separated by certain distances from the equatorial layer line at the center. With a calibration-free intrinsic layer line-distance method,[52] the chiral indices (n,m) of the nanotube can then be determined without ambiguity.

Figure 1 presents the chirality distribution of sample S1 based on ED analysis of a total of 166 individual SWCNTs. For clarity, only SWCNTs with an occurrence rate over 2% are presented in the histogram. Figure 1 reveals that the sample S1 shows a very narrow (n,m) distribution with a preference for nanotubes near the armchair region, with (11,9) being the most abundant chiral species with a concentration of about 17%. Additionally, the nanotube diameter distribution falls into a narrow range of 1.2−1.5 nm, and M% is about 24%. In the S2 sample,[48] a wider chirality distribution with a total of 49 types of chiralities has been identified among all 90 observed SWCNTs, and M% is about 33%. In the case of the RM8281 sample,[49] ED analysis of about 90 individual nanotubes indicates that (6,5) nanotube is the most abundant chirality with a concentration about 24% and M% is determined to be about 21%.

Evaluating M% of SWCNT Samples Based on Raman Spectroscopy. Currently there are two commonly used strategies for quantitative evaluation of M% in SWCNT samples. The first strategy employs the integrated intensities of RBMs (I_{RBM}) in the Raman spectra.[9,18−24] The fractions of M- and S-SWCNT in a sample are assumed to be proportional to their integral RBM intensities in the M- and S-SWCNT regions of a Raman spectrum, respectively. Then the M% of a sample is calculated by comparing the intensity ratio of RBMs in the M-SWCNT region to that in the S-SWCNT region (I^{M}_{RBM}/I^{S}_{RBM}) with such a ratio of a reference sample with known M%. This approach is often employed in bulk SWCNT samples (e.g., network-type thin films,[19] arrays,[18] forests,[22] and suspensions[23]) with diameter distributions within 0.8−1.9 nm.

The second strategy counts the numbers (n) of RBM peaks in the Raman spectral mapping.[25−33] The M% at each E_{Laser} is directly calculated by statistically counting the numbers of RBM peaks in the M- and S-SWCNT regions of a series of micro-Raman spectra acquired by Raman spectral mapping, that is, $M\% = \frac{n_{M\text{-}SWCNT}}{n_{S\text{-}SWCNT} + n_{M\text{-}SWCNT}} \times 100\%$ This procedure needs sparse SWCNT samples on a substrate.

Evaluation of M% by Integrating RBM Intensities. Resonant Raman spectrum of the HiPCO sample presents RBMs in a wide range of 190−300 cm^{-1}, corresponding to both S- and M-SWCNTs under excitation wavelengths (λ_{Laser}) of 488, 514, 633 nm. Since the first strategy requires a reference SWCNT sample with known M%, usually commercial HiPCO SWCNT samples, with an estimated M% of about 36% (±4%),[9,18−20,23] are employed as the reference sample. Figure 2 shows Raman spectra of the HiPCO and S1 samples excited by (a) 633, (b) 514, (c) 488, and (d) 785 nm lasers, respectively. The RBMs of a HiPCO sample under four excitations are located in the range of about 190−300 cm^{-1}, which is in good agreement with its diameter distribution of 0.8−1.2 nm, subject to the inverse relationship between RBM frequency and nanotube diameter.[6] Compared with the *Kataura* plot[54,55] (Figure 3) that plots optical transition energies of each (n,m) against the RBM frequencies, the observed RBMs can be assigned to electronic types (S- or M-SWCNTs) or even to specific chiralities. Details description of this *Kataura* plot is provided in the Supporting Information. We have previously calibrated and tested the *Kataura* plot used here using the ED technique.[49,56] It can be observed in Figure 3 that the RBMs of the HiPCO sample correspond to both M- and S-SWCNTs at λ_{Laser} = 633, 514, and 488 nm but to only S-SWCNTs at λ_{Laser} = 785 nm. Thus, the 785 nm laser is not applicable for the M% calculation, since the RBM intensity ratio I^{M}_{RBM}/I^{S}_{RBM} of the HiPCO sample is 0, which leads to the calculated M% to be 100% for any SWCNT sample. Because of this apparently biased evaluation, the other three λ_{Laser} (488, 514, and 633 nm) are more favored for M% calculation in the literature.[9,18−20,23]

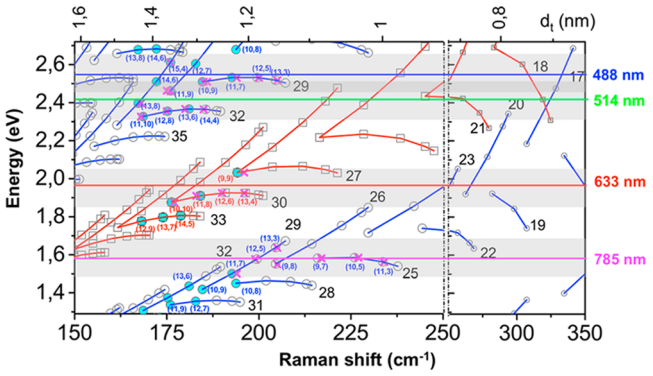

Figure 3. Enlarged *Kataura* plot in the range of 150−250 cm^{-1} (left) and 250−350 cm^{-1} (right). For comparison, both the chirality (n,m) of an S1 sample measured from ED and (n,m) assignments based on RBM Raman features at λ_{Laser} = 488, 514, 633, and 785 nm are indicated in the plot using the filled blue dots and pink crosses, respectively. The light gray squares indicate the resonance window widths of 100 meV with E_{Laser} as the centerline.

The M% of sample S1, calculated based on integrated Raman RBM intensities, largely depends on the applied E_{Laser} due to its diameter distribution. Compared to the RBM features of the HiPCO sample, S1 possesses a much narrower diameter distribution of 1.2−1.5 nm, leading to a significantly narrower range of RBMs positioned at a lower frequency of 170−200 cm^{-1} at excitations of 633, 514, and 488 nm. This narrow range of RBMs, as shown in the enlarged *Kataura* plot (Figure 3), corresponds to mainly M-SWCNTs at λ_{Laser} = 633 nm, while exclusively S-SWCNTs at λ_{Laser} = 488 and 514 nm. Meanwhile, the Raman feature of the G^{-} band of sample S1 shows the expected features, that is, a broad Breit-Wigner-Fano (BWF) shape at λ_{Laser} = 633 nm (Figure 2a), indicating the dominant resonant M-SWCNTs,[17,57] and a Lorentzian symmetric shape at λ_{Laser} = 514 nm (Figure 2b) corresponding to the resonant S-SWCNTs. When utilizing λ_{Laser} of 785 nm, similarly as in the case of the HiPCO sample, only S-SWCNTs of S1 are in

DOI: 10.1021/acs.analchem.7b03712
Anal. Chem. 2018, 90, 2517−2525

resonance, while the RBM frequencies of S1 are located at relatively lower frequencies of 200−230 cm^{-1} due to the larger diameter distribution compared to the HiPCO sample. To quantify the M% of S1, we integrated the intensities of RBMs at λ_{Laser} of 633, 514, and 488 nm, respectively, which results in an extremely high evaluated M% of 92−93% at λ_{Laser} = 633 nm but 0% when λ_{Laser} = 488 and 514 nm. On the contrary, ED measurements yield a M% of 24%. From the above results, it is clear that the M% evaluated based on Raman RBM intensity analysis at several discrete λ_{Laser} (E_{Laser}) is problematic. Because of the fact that diameter distribution of SWCNTs determines the range of RBM frequencies, the resonant M- or S-SWCNTs are then decided by the employed E_{Laser}, as indicated in the *Kataura* plot. This significant variance in RBM frequencies resulted from diameter and E_{Laser}, will finally lead to large discrepancies in the calculated M% values.

These dependencies of RBM intensities on diameter and E_{Laser} are further confirmed by Raman spectra of the S2 and RM8281 samples, as shown in Figures S2 and S3 (Supporting Information), respectively. First, the S2 SWCNTs possess a very similar diameter distribution (0.8−1.4 nm) compared to the HiPCO reference sample (0.8−1.2 nm). However, the presence of nanotubes with a larger diameter in S2 results in much higher integrated intensities of RBMs at lower frequencies that correspond to M-SWCNTs at λ_{Laser} = 633 nm and S-SWCNTs at λ_{Laser} = 514 and 488 nm. Therefore, the estimated M% of S2 is over 50% at λ_{Laser} = 633 nm but becomes as low as 3% at λ_{Laser} = 488 and 514 nm. In contrast, ED measurements of M% in the S2 sample results in about 33%. Second, in the case of the RM8281 reference material released by NIST, we measured the (*n*,*m*) distribution by both ED and optical absorption measurements, which revealed that the (6,5) nanotube is the major chirality. However, it is not at all detected by Raman spectroscopy at λ_{Laser} = 488 and 785 nm. At λ_{Laser} = 514 and 633 nm, only minor RBM peaks were observed in the Raman spectra due to the weak resonance of the (6,5) tube with the excitation energy.

Further, using SWCNT samples with known (*n*,*m*) distributions obtained by ED analysis, we explore the sources of uncertainty in an RBM intensity analysis. As shown in Figure 4, the (*n*,*m*) assignments are given in the RBM Raman spectra of the S1 sample using a sum of Lorentzian fitting under λ_{Laser} = 488, 514, 633, and 785 nm. The experimental fitting results with comparisons of theoretical (*n*,*m*) assignments are listed in Table S1 in the Supporting Information. For a straightforward comparison, both (*n*,*m*) assignments based on ED (filled blue dots) and on Raman spectra (pink crosses) are shown in the *Kataura* plot (Figure 3), respectively. A typical resonance window of 100 meV[17] is employed for the SWCNT network films studied here, which is indicated as a filled light gray area with the E_{Laser} as a center line, as shown in Figure 3. This means that the SWCNTs with transition energies within E_{Laser} ± 100 meV are all considered for (*n*,*m*) assignments.

The RBM intensity of a SWCNT largely depends on the match of E_{ii} with E_{Laser}. The ED measurements of S1 show that the (11,9) tube is the most abundant nanotube with a concentration of 17%, while the (10,9) tube shows 11%. However, in the Raman spectra obtained at λ_{Laser} = 488 nm (Figure 4a), the intensity of RBM from the (10,9) tubes is much stronger than that from the (11,9) tubes, even when accounting for the possibility of additional contributions from (15,4) tubes to the same RBM peak assigned to the (11,9) nanotube. One of the reasons is clearly implied in the *Kataura* plot: the E_{33}^{S} transition (2.51 eV) of the (10,9) tube matches the E_{Laser} of 488 nm (2.54 eV) significantly better than that (2.46 eV) of the (11,9) tube, and the RBM intensity of a SWCNT is a function of E_{Laser} and achieves sharp maxima when E_{Laser} equals an optical transition energy E_{ii}.[58] Such E_{Laser} dependence in the RBM intensity is also observed in Raman spectra at λ_{Laser} = 633 and 785 nm, as shown in Figure 4c,d, respectively. A detailed description is provided in the Supporting Information.

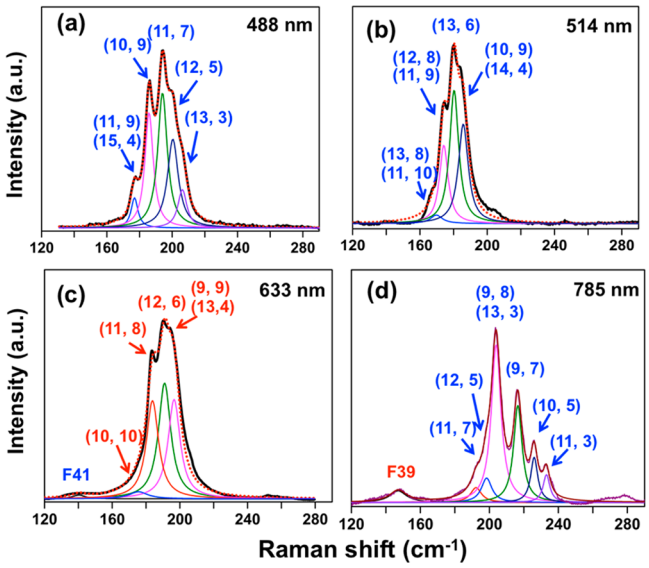

Figure 4. RBM Raman spectra of S1 sample at λ_{Laser} of (a) 488, (b) 514, (c) 633, and (d) 785 nm, respectively. The (*n*,*m*) assignments are given in the RBM Raman spectra after the Lorentzian spectral fitting, and the family (2*n* + *m*) assignments are denoted as F. The assignments in blue and red color indicate the S- and M-SWCNTs, respectively.

Interestingly, when we reverse the resonance condition of (11,9) and (10,9) tubes by utilizing the 514 nm (2.41 eV) laser, we observed the same phenomenon as when using the 488 nm (2.54 eV) laser. The RBM intensity from (10,9) tubes is stronger than that from (11,9) tubes, although the E_{33}^{S} of (11,9) tubes is now much better matched with the E_{Laser} than that of (10,9) tubes. As seen in Figure 4b, the RBM at 175 cm^{-1}, with a relatively weak intensity is assigned to (11,9) and (12,8) tubes with a total concentration of 24%. However, the RBM at 185 cm^{-1}, with a relatively strong intensity results from (10,9) and (14,4) tubes with a total concentration of 11%. Therefore, causes different from the underlying (*n*,*m*) abundance and matching of E_{ii} with E_{Laser} should be responsible for the relatively high intensity of RBM from (10,9).

We ascribe this behavior to a strong *mod* type dependence of the RBM intensity, as predicted by theory.[34] Previous theoretical predictions[34,43,44,59] have shown the significant dependences of RBM intensity on the nanotube *mod* type (*mod* = 0, 1, 2), diameter d_t, chiral angle θ, and resonance transition energy E_{ii}. In the current measurement, we can exclude diameter, chiral angle, and resonant transition energy related variations of RBM Raman intensity since (10,9) and (11,9) nanotubes are at the same resonance excitation of E_{33} by using λ_{Laser} = 514 and 488 nm and possess about the same d_t of 1.29 and 1.36 nm, and θ of 28° and 27°, respectively. However, the different *mod* type of (10,9) and (11,9) nanotubes, *mod1* and *mod2*, respectively, has been predicted to considerably

DOI: 10.1021/acs.analchem.7b03712
Anal. Chem. 2018, 90, 2517−2525

affect their optical properties,[58,60] since *mod1* and *mod2* semiconducting nanotubes position their transition energies E_{ii} at opposing sides with respect to the K point in the reciprocal space. The exciton−phonon coupling strengths have been predicted to be very different near the vicinity of the K point, which dominates the variations in Raman intensity.[34,43,44,59] Recently, Piao et al. published experiments[46] on single-chirality-enriched S-SWCNTs, which have shown that *mod2* tubes exhibit an overall higher RBM intensity than that of *mod1* tubes under a Raman excitation matching with E_{22}. They observed that the intensity ratio of RBM to G^+ mode of (8,3) tubes (*mod2*) is nearly 500 times larger than that of (8,4) tubes (*mod1*). Since the E_{22} and E_{33} of a nanotube are on opposing sides of the K point, *mod2* nanotubes, which display a strong RBM signal when excited at E_{22}, are expected to show a weak signal when excited at E_{33}. This agrees very well with our observation that (11,9) (*mod2*) tubes exhibit much weaker RBM intensity than (10,9) (*mod1*) tubes when excited at E_{33}, regardless of their higher concentration in S1 and even though their E_{33} better matches with E_{Laser}.

We can thus conclude that quantitative or even qualitative evaluation of M% in a SWCNT sample based on RBM intensities measured at discrete laser wavelengths is misrepresentative. This misrepresentation is first due to the strict inverse relationship between RBM frequency and d_t of a nanotube, the frequencies of RBMs corresponding to M- or S-SWCNTs in a Raman spectrum can be predicted by their diameter distribution and applied laser energy but are not proportional to M% or S%. Also one remarkable peculiarity of Raman scattering from SWCNTs is the dependence of Raman intensity (particularly the RBM feature) on E_{Laser} in the vicinity of their transition energies.[17] Further the RBM intensity of SWCNTs is highly dependent on (n,m) because of their different exciton−phonon coupling strengths. Therefore, the integrated RBM intensities measured by several discrete E_{Laser} depend strongly on the diameter distribution, applied E_{Laser}, and RBM cross-sections of each (n,m) and thereby cannot be reliably used to assess the M% or S% in a SWCNT sample.

As a solution for the issues described above, by using continuous excitation energies in a wide range, Raman spectroscopy could efficiently detect all (n,m) nanotubes in a sample. Meanwhile, the dependence of RBM intensity on E_{Laser} could be eliminated by fitting Raman excitation profiles (a plot of Raman intensity as a function of E_{Laser}) for the maximum RBM intensity of a certain type of chirality. If theoretical corrections for the (n,m)-related influence on RBM intensity,[34,36,39,41,43,44,59] as well as environmental effects,[37,61] are taken into consideration, RBM intensities would be exclusively determined by (n,m) concentrations in a sample and thus the corrected maximum RBM intensities could be used to calculate M%.

Evaluation of M% by Counting RBM Peak Numbers. Because of the apparent drawbacks of the first strategy based on integrated RBM intensities, it has become fashionable to use the second strategy of calculating M% by statistically counting the numbers of RBM features appearing in the M- or S-SWCNT regions of a series of micro-Raman spectra acquired by Raman spectral mapping.[10,11,25−33] Typically, two[26,33] to six[11] different E_{Laser} have been utilized to calculate the M% of a SWCNT sample. Because of the nature of this method, sparsely distributed SWCNT samples on a substrate are needed. We deposited an S1 sample on a SiO_2/Si chip directly from the FC-CVD reactor with a density of ~2 tubes/μm^2, as shown in the SEM image (Figure 5a). The Raman spectral mapping, consisting of 256 micro-Raman spectra of the S1 sample at four different E_{Laser}, is shown in Figure 5b−e.

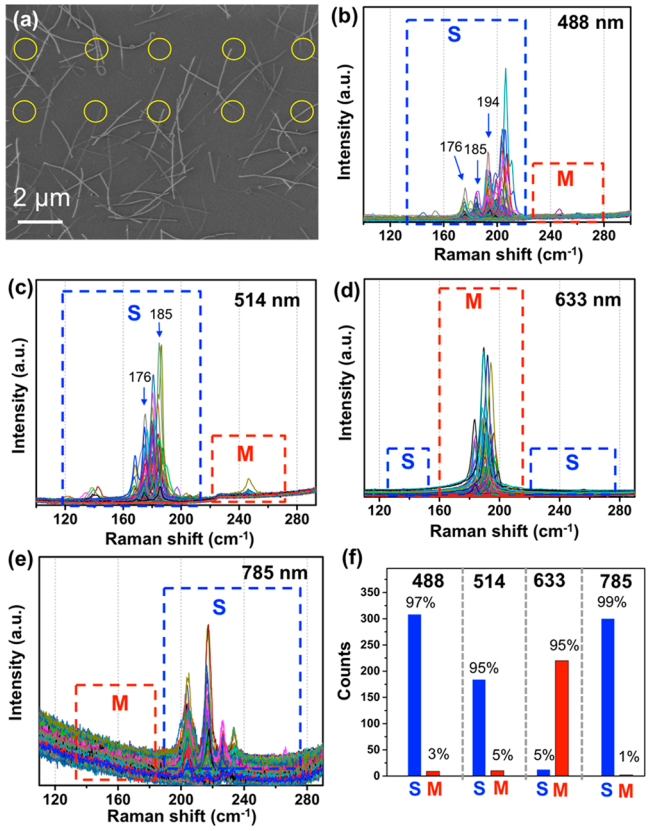

Figure 5. (a) SEM image of the S1 sample on Si/SiO_2 substrate. The yellow circles demonstrate the laser spot size of 1 μm that scans over an area of 60 × 60 μm^2 with a scanning step of 4 μm. (b−e) Series of micro-Raman spectra of Raman spectral mapping measured from the S1 on substrate using λ_{Laser} = 488, 514, 633, and 785 nm lasers, respectively. (f) Calculated M% and S% of S1 sample by statistically counting the occurrences of RBMs in the regions of Raman spectral mapping assignable to M- and S-SWCNTs.

The M% of S1, evaluated by statistically counting the occurrences of RBMs in Raman spectral mapping, is very similar to M% calculated from integrated RBM intensities at each E_{Laser}. It is observed that the isolated individual S1 nanotubes or small bundles on substrate exhibit RBM peaks with much narrower peak widths compared to the RBMs measured from the network film sample (Figure 2), while the RBM frequencies are located in a very similar wavenumber range of 170−200 cm^{-1} due to the same d_t distribution. This range of RBMs corresponds to M-SWCNTs at 633 nm and S-SWCNTs at 488, 514, and 785 nm excitations. Therefore, similarly to the M% values calculated from integrated RBM intensities, the statistical count of the number of RBM features in the M- and S-SWCNT regions of 256 micro-Raman spectra at each E_{Laser} yields an extremely high M% of 95% at 633 nm but very low values of 3%, 5%, and 1% at 488, 514, and 785 nm lasers (Figure 5f), respectively.

The final average M% of a sample is dependent on the quantity and excitation energies of the applied lasers. In the literature, two[26,33] to six[11,32] different lasers have been utilized to calculate the M% of a SWCNT sample by averaging the

DOI: 10.1021/acs.analchem.7b03712
Anal. Chem. 2018, 90, 2517−2525

values of M% obtained at different E_{Laser}. Here, if two or three E_{Laser} were applied, the calculated M% of S1 can vary from 2% to 50% and 3% to 34%, respectively, depending on the specific combination of E_{Laser}. Averaging all four E_{Laser} gives a M% of 26%. Notably, increasing the number of different E_{Laser} does not simply lead to a more accurate result. For example, the calculated M% of S1 will increase if the applied E_{Laser} is close to 633 nm (1.96 eV), that is, mainly resonant with M-SWCNTs of S1 and decrease when E_{Laser} predominantly matches with E_{ii} of S-SWCNTs.

One of the reasons for the large variance in the obtained M% is that several laser lines do not efficiently detect most (n,m) in a SWCNT sample. As indicated in the (n,m) distribution of S1 measured by ED, the M-SWCNTs with percentage higher than 2% are (10,10) (6%), (11,8) (5%), (13,7) (4%), (12,9) (4%), (9,9) (2%), and (14,5) (2%) (with diameters within 1.2−1.5 nm). However, among these M-SWCNTs, only (10,10), (11,8), and (9,9) tubes are detected by 633, 514, 488, and 785 nm lasers (as indicated in the *Kataura* plot in Figure 3), and thus the four excitation energies used can only excite ∼50% of M-SWCNTs in S1. Because of such partial detection, even when employing multiple E_{Laser}, it is difficult to reflect the full contents of a SWCNT sample using Raman spectra. By using prior knowledge of the diameter distribution obtained by, e.g., optical absorption spectroscopy, one can roughly select the appropriate E_{Laser} to excite the nanotubes. The (n,m) distribution, that is, whether their E_{ii} match with E_{Laser} or not, is another important parameter that determines the detectable percentage of a SWCNT sample.

Meanwhile, if the applied excitation energies are too close, nanotubes with (n,m) resonant with all the E_{Laser} will be multiply counted. As an example, in the present work, the predominant chiralities of (11,9) and (10,9) tubes in S1 are resonant with both λ_{Laser} = 488 and 514 nm and exhibit RBMs at 176 and 185 cm^{-1} (as indicated in Figure 5b,c), respectively. Consequently the semiconducting nanotubes of (11,9) and (10,9) are double counted when calculating M%, which obviously causes ambiguity in the final results. Therefore, without prerequisites of the examined samples, it is practically hard to make a proper selection of a resonance window, that is, the energy interval of discrete laser lines, to avoid multiple counting or missing counts of the nanotubes.

Further, we observe an unforeseen phenomenon: the occurrence number of an RBM peak is not a simple function of the underlying (n,m) concentration. As shown in Figure 5b, when excited by 488 nm laser, the RBMs at 176 cm^{-1} can be assigned to (15,4) and (11,9) tubes, and the RBMs at 185 and 194 cm^{-1} correspond to (10,9) and (11,7) nanotubes, respectively. The statistic count of numbers of RBM peaks located at 176, 185, and 194 cm^{-1} are 23, 59 and 73, respectively, in the 256 micro-Raman spectra obtained at λ_{Laser} = 488 nm. Within these four chiralities, the (11,7) tubes (RBM at ≈194 cm^{-1}) with minimal concentration of 4% exhibit the largest occurrence of 73 times in the micro-Raman spectra, while the most abundant nanotubes of (11,9) and (15,4) (RBM at ≈176 cm^{-1}), with a total concentration of 18%, are only present 23 times and (10,9) tubes (RBM at ≈184 cm^{-1}) with a concentration of 11% are present 59 times.

Similar to the RBM intensity, we find that the occurrence frequency of RBMs in Raman spectral mapping largely depends on the resonant coupling degrees between E_{ii} and E_{Laser} as well as the chiral index (n,m). In the Raman spectral mapping measurement of isolated and individual or bundled SWCNTs on a substrate, only a few nanotubes either in part or completely, are under the laser spot at each measurement point and contribute to a micro-Raman spectrum. Thus, nanotubes of chiralities with larger RBM cross sections and strongly at resonance with the applied E_{Laser} possess a larger probability to exhibit a distinguishable RBM feature above the noise, which results in a higher number of occurrences in the statistical evaluation of hundreds of micro-Raman spectra. For example, the (11,7) chirality exhibits the highest number of observed RBM peaks in the 256 micro-Raman spectra obtained at a wavelength of 488 nm, despite its relatively low concentration in S1, since its E_{33} of 2.53 eV is the most accurate match with the E_{Laser} of 2.54 eV, when compared to other resonant chiralities. Meanwhile, (11,7) tubes, of the *mod2* type, exhibit a much stronger Raman signal than that of *mod1* type S-SWCNTs (e.g., (11,9) and (15,4)) when excited to E_{33}, due to the variations in exciton−phonon coupling strength. Therefore, the count of observed RBM peaks in Raman spectral mapping assignable to a particular (n,m) is not simply proportional to its abundance but essentially associates to the specific E_{ii} in resonance with E_{Laser} and the RBM cross-section.

In recent years, the second strategy of employing RBM peak numbers is much more accepted and employed than the first method of using integrated RBM intensities to evaluate the M% of a SWCNT sample. It is generally believed that the numbers (the occurrence frequencies) of RBMs appearing in Raman spectral mapping represent the numbers (concentrations) of corresponding (n,m) nanotubes on the substrate and thereby can be directly used to calculate the M% or even (n,m) population in a SWCNT sample. However, our results disclose a number of comprehensive factors affecting the RBM peak numbers that occur in Raman spectral mapping. Ideally, to validate the second strategy for the accurate calculation of M% of a SWCNT sample, one first needs to carefully select the range of multiple laser excitation energies to efficiently detect most of (n,m) in a SWCNT. In addition, appropriate energy intervals of E_{Laser} have to be considered to avoid either undetected tubes or multiple counts of the same tube. (n,m)-associated Raman scattering cross sections and environmental influences should also be taken into account for the quantitative calculations. Notably, all above-mentioned factors are correlated to the (n,m) distribution of a SWCNT sample. Thus, in practical measurements, the validation of this strategy for a (n,m)-distribution-unknown sample remains an open question.

CONCLUSIONS

To summarize, in this work, we comprehensively examine the validity of the quantitative evaluation of M% on the basis of Raman spectroscopy. For this purpose, three SWCNT samples with different diameter and chirality distributions were employed for Raman spectroscopy measurements at λ_{Laser} of 488, 514, 633, and 785 nm. To evaluate the results of Raman measurements, all three samples were analyzed with an advanced calibration-free ED technique, giving reliable (n,m) distributions. Our results show that quantitative Raman evaluations M% at multiple discrete E_{Laser} either (1) by using integrated intensities of RBMs or (2) by statistically counting the numbers of (n,m)-associated RBMs is misrepresentative. The occurrence of RBMs in the regions of Raman spectra assignable to M- and S-SWCNTs at discrete laser lines depends largely on the diameter distribution of the SWCNT sample; this is because of the relationship between diameter and the RBM frequency. Neither the intensities nor the occurrence

DOI: 10.1021/acs.analchem.7b03712
Anal. Chem. 2018, 90, 2517−2525

numbers of RBMs assignable to M- or S-SWCNTs is directly proportional to the underlying M- or S-SWCNT abundance. In addition, we found for the first time that the occurrence numbers of RBMs in Raman spectral mapping depend significantly on the resonant coupling degrees between E_{ii} and E_{Laser} as well as the (n,m)-related RBM cross sections. These dependencies are similar to that observed in the integrated intensities of RBMs. Furthermore, our results provide strong experimental evidence of important *mod* type dependence of the RBM intensity in larger diameter nanotubes (d_t > 1.3 nm). Though the dependence of Raman intensity on chiral structure of nanotube has been recognized early, this work advances the understanding of using Raman spectroscopy for quantitative analysis of carbon nanotube samples and arouses our awareness of pitfalls associated with this method, thus paving the way to reliable measurements of M- and S-SWCNT fractions with quantitative Raman spectroscopy.

■ ASSOCIATED CONTENT

Supporting Information

The Supporting Information is available free of charge on the ACS Publications website at DOI: 10.1021/acs.analchem.7b03712.

High-resolution TEM image and the corresponding ED pattern of the S1 sample, RBM Raman spectra of the S2 and HiPCO SWCNT samples and the NIST RM8281 standard SWCNT sample, detailed description of the fitting process of RBM Raman spectra and the theoretical *Kataura* plot, table of (n,m) assignments of the S1 sample, and detailed analysis of association of RBM intensities with (n,m) abundance of the S1 sample at 633 and 785 nm excitations (PDF)

■ AUTHOR INFORMATION

Corresponding Authors

*E-mail: tianying@dlmu.edu.cn. Phone: +86 15524691391.
*E-mail: hua.jiang@aalto.fi. Phone: +358 505942367.

ORCID

Ying Tian: 0000-0002-8841-9185
Patrik Laiho: 0000-0001-8234-1607

Notes

The authors declare no competing financial interest.

■ ACKNOWLEDGMENTS

This work was funded by National Natural Science Foundation of China (Grant 51502031), Academy of Finland (Grant 276160), TEKES Project CARLA, JST-EC DG RTD Coordinated Research Project IRENA, Fundamental Research Funds for the Central Universities of China (Grants 3132017066 and 3132016349), and Application Foundation (Main subject) of Ministry of Transport of China (Grant 2015329225090). This work made use of the Aalto University Nanomicroscopy Center (Aalto-NMC) premises.

■ REFERENCES

(1) Odom, T. W.; Huang, J.-L.; Kim, P.; Lieber, C. M. *Nature* **1998**, *391*, 62−64.
(2) Tans, S. J.; Verschueren, A. R. M.; Dekker, C. *Nature* **1998**, *393*, 49−52.
(3) Shulaker, M. M.; Hills, G.; Patil, N.; Wei, H.; Chen, H.-Y.; Wong, H. S. P.; Mitra, S. *Nature* **2013**, *501*, 526−530.
(4) Sun, D.-m.; Timmermans, M. Y.; Tian, Y.; Nasibulin, A. G.; Kauppinen, E. I.; Kishimoto, S.; Mizutani, T.; Ohno, Y. *Nat. Nanotechnol.* **2011**, *6*, 156−161.
(5) Liu, C.; Cheng, H.-M. *J. Am. Chem. Soc.* **2016**, *138*, 6690−6698.
(6) Riichiro, S.; Gene, D.; Mildred, S. D. *Physical Properties of Carbon Nanotubes*; World Scientific: London, U.K., 1998.
(7) Yao, Z.; Kane, C. L.; Dekker, C. *Phys. Rev. Lett.* **2000**, *84*, 2941.
(8) Dai, H.; Wong, E. W.; Lieber, C. M. *Science* **1996**, *272*, 523.
(9) Harutyunyan, A. R.; Chen, G.; Paronyan, T. M.; Pigos, E. M.; Kuznetsov, O. A.; Hewaparakrama, K.; Kim, S. M.; Zakharov, D.; Stach, E. A.; Sumanasekera, G. U. *Science* **2009**, *326*, 116−120.
(10) Zhang, S.; Kang, L.; Wang, X.; Tong, L.; Yang, L.; Wang, Z.; Qi, K.; Deng, S.; Li, Q.; Bai, X.; Ding, F.; Zhang, J. *Nature* **2017**, *543*, 234−238.
(11) Yang, F.; Wang, X.; Zhang, D.; Yang, J.; Luo, D.; Wei, J.; Wang, J.-Q.; Xu, Z.; Peng, F.; Li, X.; Li, R.; Li, Y.; Li, M.; Bai, X.; Ding, F.; Li, Y. *Nature* **2014**, *510*, 522−524.
(12) Yu, B.; Liu, C.; Hou, P.-X.; Tian, Y.; Li, S.; Liu, B.; Li, F.; Kauppinen, E. I.; Cheng, H.-M. *J. Am. Chem. Soc.* **2011**, *133*, 5232−5235.
(13) He, M.; Jiang, H.; Liu, B.; Fedotov, P. V.; Chernov, A. I.; Obraztsova, E. D.; Cavalca, F.; Wagner, J. B.; Hansen, T. W.; Anoshkin, I. V. *Sci. Rep.* **2013**, *3*, 1460.
(14) Ghosh, S.; Bachilo, S. M.; Weisman, R. B. *Nat. Nanotechnol.* **2010**, *5*, 443−450.
(15) Tu, X.; Manohar, S.; Jagota, A.; Zheng, M. *Nature* **2009**, *460*, 250−253.
(16) Zheng, M.; Jagota, A.; Semke, E. D.; Diner, B. A.; McLean, R. S.; Lustig, S. R.; Richardson, R. E.; Tassi, N. G. *Nat. Mater.* **2003**, *2*, 338−342.
(17) Dresselhaus, M. S.; Dresselhaus, G.; Saito, R.; Jorio, A. *Phys. Rep.* **2005**, *409*, 47−99.
(18) Qu, L.; Du, F.; Dai, L. *Nano Lett.* **2008**, *8*, 2682−2687.
(19) Chiang, W.-H.; Sakr, M.; Gao, X. P. A.; Sankaran, R. M. *ACS Nano* **2009**, *3*, 4023−4032.
(20) Sakurai, S.; Yamada, M.; Sakurai, H.; Sekiguchi, A.; Futaba, D. N.; Hata, K. *Nanoscale* **2016**, *8*, 1015−1023.
(21) Fouquet, M.; Bayer, B. C.; Esconjauregui, S.; Thomsen, C.; Hofmann, S.; Robertson, J. *J. Phys. Chem. C* **2014**, *118*, 5773−5781.
(22) Ohashi, T.; Iwama, H.; Shima, T. *J. Appl. Phys.* **2016**, *119*, 084303.
(23) Krupke, R.; Hennrich, F.; Löhneysen, H. v.; Kappes, M. M. *Science* **2003**, DOI: 10.1002/chin.200343198.
(24) Ding, L.; Tselev, A.; Wang, J.; Yuan, D.; Chu, H.; McNicholas, T. P.; Li, Y.; Liu, J. *Nano Lett.* **2009**, *9*, 800−805.
(25) Zhang, F.; Hou, P.-X.; Liu, C.; Wang, B.-W.; Jiang, H.; Chen, M.-L.; Sun, D.-M.; Li, J.-C.; Cong, H.-T.; Kauppinen, E. I.; Cheng, H.-M. *Nat. Commun.* **2016**, *7*, 11160.
(26) Zhang, S.; Tong, L.; Hu, Y.; Kang, L.; Zhang, J. *J. Am. Chem. Soc.* **2015**, *137*, 8904−8907.
(27) Hong, G.; Zhang, B.; Peng, B.; Zhang, J.; Choi, W. M.; Choi, J.-Y.; Kim, J. M.; Liu, Z. *J. Am. Chem. Soc.* **2009**, *131*, 14642−14643.
(28) An, H.; Kumamoto, A.; Takezaki, H.; Ohyama, S.; Qian, Y.; Inoue, T.; Ikuhara, Y.; Chiashi, S.; Xiang, R.; Maruyama, S. *Nanoscale* **2016**, *8*, 14523−14529.
(29) Kang, L.; Zhang, S.; Li, Q.; Zhang, J. *J. Am. Chem. Soc.* **2016**, *138*, 6727−6730.
(30) Li, P.; Zhang, J. *J. Mater. Chem.* **2011**, *21*, 11815−11821.
(31) Yang, F.; Wang, X.; Zhang, D.; Qi, K.; Yang, J.; Xu, Z.; Li, M.; Zhao, X.; Bai, X.; Li, Y. *J. Am. Chem. Soc.* **2015**, *137*, 8688−8691.
(32) Yang, F.; Wang, X.; Si, J.; Zhao, X.; Qi, K.; Jin, C.; Zhang, Z.; Li, M.; Zhang, D.; Yang, J.; Zhang, Z.; Xu, Z.; Peng, L.-M.; Bai, X.; Li, Y. *ACS Nano* **2017**, *11*, 186−193.
(33) Qin, X.; Peng, F.; Yang, F.; He, X.; Huang, H.; Luo, D.; Yang, J.; Wang, S.; Liu, H.; Peng, L.; Li, Y. *Nano Lett.* **2014**, *14*, 512−517.
(34) Popov, V. N.; Henrard, L.; Lambin, P. *Nano Lett.* **2004**, *4*, 1795−1799.
(35) Shreve, A. P.; Haroz, E. H.; Bachilo, S. M.; Weisman, R. B.; Tretiak, S.; Kilina, S.; Doorn, S. K. *Phys. Rev. Lett.* **2007**, *98*, 037405.

(36) Jiang, J.; Saito, R.; Grüneis, A.; Chou, S. G.; Samsonidze, G. G.; Jorio, A.; Dresselhaus, G.; Dresselhaus, M. S. *Phys. Rev. B: Condens. Matter Mater. Phys.* **2005**, *71*, 205420.
(37) Ghosh, S.; Wei, F.; Bachilo, S. M.; Hauge, R. H.; Billups, W. E.; Weisman, R. B. *ACS Nano* **2015**, *9*, 6324−6332.
(38) Piao, Y.; Meany, B.; Powell, L. R.; Valley, N.; Kwon, H.; Schatz, G. C.; Wang, Y. *Nat. Chem.* **2013**, *5*, 840−845.
(39) Maultzsch, J.; Telg, H.; Reich, S.; Thomsen, C. *Phys. Rev. B: Condens. Matter Mater. Phys.* **2005**, *72*, 205438.
(40) Popov, V. N.; Henrard, L.; Lambin, P. *Phys. Rev. B: Condens. Matter Mater. Phys.* **2005**, *72*, 035436.
(41) Jorio, A.; Fantini, C.; Pimenta, M. A.; Capaz, R. B.; Samsonidze, G. G.; Dresselhaus, G.; Dresselhaus, M. S.; Jiang, J.; Kobayashi, N.; Grüneis, A. *Phys. Rev. B: Condens. Matter Mater. Phys.* **2005**, *71*, 075401.
(42) Yin, Y.; Vamivakas, A. N.; Walsh, A. G.; Cronin, S. B.; Ünlü, M. S.; Goldberg, B. B.; Swan, A. K. *Phys. Rev. Lett.* **2007**, *98*, 037404.
(43) Machón, M.; Reich, S.; Telg, H.; Maultzsch, J.; Ordejón, P.; Thomsen, C. *Phys. Rev. B: Condens. Matter Mater. Phys.* **2005**, *71*, 035416.
(44) Goupalov, S. V.; Satishkumar, B. C.; Doorn, S. K. *Phys. Rev. B: Condens. Matter Mater. Phys.* **2006**, *73*, 115401.
(45) Sato, K.; Saito, R.; Nugraha, A. R. T.; Maruyama, S. *Chem. Phys. Lett.* **2010**, *497*, 94−98.
(46) Piao, Y.; Simpson, J. R.; Streit, J. K.; Ao, G.; Zheng, M.; Fagan, J. A.; Hight Walker, A. R. *ACS Nano* **2016**, *10*, 5252−5259.
(47) Kaskela, A.; Laiho, P.; Fukaya, N.; Mustonen, K.; Susi, T.; Jiang, H.; Houbenov, N.; Ohno, Y.; Kauppinen, E. I. *Carbon* **2016**, *103*, 228−234.
(48) Mustonen, K.; Laiho, P.; Kaskela, A.; Zhu, Z.; Reynaud, O.; Houbenov, N.; Tian, Y.; Susi, T.; Jiang, H.; Nasibulin, A. G. *Appl. Phys. Lett.* **2015**, *107*, 013106.
(49) Tian, Y.; Jiang, H.; Anoshkin, I. V.; Kauppinen, L. J. I.; Mustonen, K.; Nasibulin, A. G.; Kauppinen, E. I. *RSC Adv.* **2015**, *5*, 102974−102980.
(50) Fagan, J. A.; Lin, N. J.; Zeisler, R.; Hight Walker, A. R. *Nano Res.* **2011**, *4*, 393−404.
(51) Krasheninnikov, A. V.; Banhart, F. *Nat. Mater.* **2007**, *6*, 723−733.
(52) Jiang, H.; Nasibulin, A. G.; Brown, D. P.; Kauppinen, E. I. *Carbon* **2007**, *45*, 662−667.
(53) Laiho, P.; Mustonen, K. A.; Ohno, Y.; Maruyama, S.; Kauppinen, E. I. *ACS Appl. Mater. Interfaces* **2017**, *9*, 20738−20747.
(54) Son, H.; Reina, A.; Samsonidze, G. G.; Saito, R.; Jorio, A.; Dresselhaus, M. S.; Kong, J. *Phys. Rev. B: Condens. Matter Mater. Phys.* **2006**, *74*, 073406.
(55) Kataura, H.; Kumazawa, Y.; Maniwa, Y.; Umezu, I.; Suzuki, S.; Ohtsuka, Y.; Achiba, Y. *Synth. Met.* **1999**, *103*, 2555−2558.
(56) Tian, Y.; Jiang, H.; Pfaler, J. v.; Zhu, Z.; Nasibulin, A. G.; Nikitin, T.; Aitchison, B.; Khriachtchev, L.; Brown, D. P.; Kauppinen, E. I. *J. Phys. Chem. Lett.* **2010**, *1*, 1143−1148.
(57) Brown, S. D. M.; Jorio, A.; Corio, P.; Dresselhaus, M. S.; Dresselhaus, G.; Saito, R.; Kneipp, K. *Phys. Rev. B: Condens. Matter Mater. Phys.* **2001**, *63*, 155414.
(58) Saito, R.; Hofmann, M.; Dresselhaus, G.; Jorio, A.; Dresselhaus, M. S. *Adv. Phys.* **2011**, *60*, 413−550.
(59) Telg, H.; Thomsen, C.; Maultzsch, J. *J. Nanophotonics* **2010**, *4*, 041660.
(60) Grüneis, A.; Saito, R.; Samsonidze, G. G.; Kimura, T.; Pimenta, M. A.; Jorio, A.; Souza Filho, A. G.; Dresselhaus, G.; Dresselhaus, M. S. *Phys. Rev. B: Condens. Matter Mater. Phys.* **2003**, *67*, 165402.
(61) Kwon, H.; Kim, M.; Meany, B.; Piao, Y.; Powell, L. R.; Wang, Y. *J. Phys. Chem. C* **2015**, *119*, 3733−3739.

DOI: 10.1021/acs.analchem.7b03712
Anal. Chem. 2018, 90, 2517−2525